SINGLE-SAMPLE DIRECTION-OF-ARRIVAL ESTIMATION FOR FAST AND ROBUST 3D LOCALIZATION WITH REAL MEASUREMENTS FROM A MASSIVE MIMO SYSTEM

Stepan Mazokha, Sanaz Naderi, Georgios I. Orfanidis, George Sklivanitis, Dimitris A. Pados and Jason O. Hallstrom

Center for Connected Autonomy and AI
Institute for Sensing and Embedded Network Systems Engineering
Florida Atlantic University Boca Raton, FL, 33431, USA
E-mail: {smazokha2016, snaderi2021, gorfanidis2021, gsklivanitis, dpados, jhallstrom}@fau.edu

ABSTRACT

Fast, robust, high-accuracy localization is a key enabler for future location-aware applications in streetscape communication networks and next-generation networked autonomous agents. Specifically, massive multiple-input and multiple-output (MIMO) antenna systems have received increasing attention due to high angular resolution. However, in dense multipath environments, such as urban areas, pure direction-of-arrival (DoA)-based techniques have not been very popular due to large localization errors.

In this paper, we present and evaluate, on real measurements from the POWDER-RENEW platform, a novel method to carry out DoA estimation from just one antenna array snapshot. The measurements are taken from an indoor testbed that is based on a massive MIMO orthogonal frequency-division multiplexing (OFDM) system. Experimental results – in the presence of spatial aliasing – show that for certain emitter locations our proposed universal one-shot DoA estimator outperforms in azimuth/elevation accuracy state-of-the-art subspace-based methods that involve collection of a sufficiently large data record of antenna array snapshots.

Index Terms— Direction-of-arrival, source localization, massive MIMO, POWDER-RENEW, streetscape IoT.

1. INTRODUCTION

With the introduction of 5G and massive MIMO systems, fine-grained localization for Internet of Things and smart city applications has grown in popularity [1]. Massive MIMO systems not only benefit communications in terms of channel capacity and spectral efficiency, but also have the potential for accurate 3D localization [2]. The use of large scale arrays at 5G cellular base-stations enables estimation of new physical quantities, namely the DoA (in uplink) and angle-of-departure (AoD) (in downlink). Typically, a source emits a signal and DoA is measured at different base-stations. The source's location is found by triangulation.

Azimuth and elevation measurements [3, 4] from such systems are computationally challenging to process at scale; therefore, various techniques have been proposed to optimize DoA estimation. For instance, [5] proposes a two-stage Multiple Signal Classification (MUSIC) algorithm [6] to estimate azimuth and elevation DoAs using the rows and columns, respectively, of a 2D antenna array. Such optimization is required to avoid joint search over the 2D angular domain.

In this paper, we consider a novel single-sample DoA estimation algorithm for fast and robust 3D localization. We evaluate the proposed method on real measurements collected from a six-by-four massive MIMO uniform rectangular array (URA) deployed in the anechoic chamber of the POWDER-RENEW testbed (developed jointly with the University of Utah and Rice University). Data frames are collected over-the-air from nine different locations of an orthogonal-frequency-division multiplexing (OFDM) emitter. Data calibration and mitigation of spatial aliasing effects at the receiver array are necessary prior to using the collected measurements for 3D localization [7, 8].

Due to lack of transmitter and receiver synchronization, time, frequency, and phase offsets must be compensated prior to DoA estimation. For instance, residual drifts in the phase-locked loops of each RF chain at the receiver antenna array introduce carrier frequency offsets, which cause the receiver's center frequency to drift relative to the carrier frequency of the emitter [7, 9]. Since the time of each transmitted OFDM symbol is not known at the receiver, symbol time offsets are also introduced [7, 9]. Additionally, since each of the antennas in the massive MIMO system contains an independent oscillator circuit, inter-antenna phase offsets need to be calibrated as well [7, 8, 10]. Beyond DoA estimation errors due to hardware limitations, we must also deal with errors that arise due to spatial aliasing, since inter-antenna element spacing in either dimension of the URA is greater than half the wavelength of the captured signal.

In this work, upon calibration of the massive MIMO receiver measurements, we evaluate a novel approach to carry out signal DoA estimation by applying data Hankelization and singular value decomposition (SVD) to just one antenna array snapshot [11]. Historically, DoA estimation is carried out by statistical optimization methods that involve collection of a sufficiently large data record of antenna array snapshots to form an appropriate estimate of the space-domain signal autocorrelation matrix followed by vector subspace analysis techniques (e.g., MUSIC [6]). Experimental results demonstrate that for certain emitter locations, our proposed one-shot Hankel SVD method outperforms in azimuth/elevation DoA

This research is supported in part by the ERC for Smart Street Scapes, funded through NSF award EEC-2133516 and in part by NSF awards EECS-2030234, CNS-2117822, CNS-1753406, and ITE-2226392. We would also like to acknowledge POWDER-RENEW personnel Dr. Oscar Bejarano and collaborators from the Technical University of Crete, Greece, Prof. George Karystinos, and Mr. Ioannis Grypiotis for their help on data calibration.

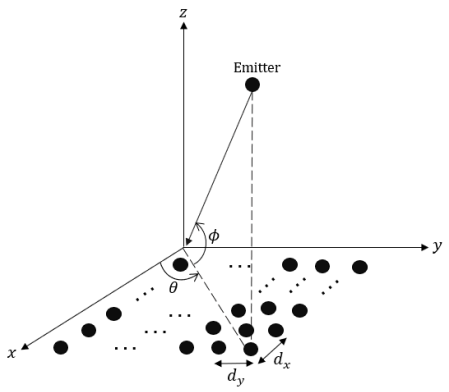

Fig. 1: Massive MIMO URA system model.

accuracy and speed the current state-of-the-art, subspace-based MUSIC, which is affected by spatial aliasing and requires a large data record.

2. SYSTEM MODEL

We consider an $M \times N$ URA (illustrated in Fig. 1), where M and N are the number of antennas in the x-axis and y-axis, respectively. Furthermore, d_x and d_y denote the distance between two subsequent elements along the x-axis and y-axis, respectively. We consider an emitter that transmits orthogonal frequency division multiplexing (OFDM) pilot frames to the URA. The received frame at the (m,n)-th antenna can be expressed as

$$\begin{aligned} y_{m,n}(i) &= h_{m,n}x(i)e^{j((m-1)\alpha+(n-1)\beta)} + n(i), \\ & i = 1,\ldots,I, \quad m = 1,\ldots,M, \quad n = 1,\ldots,N \end{aligned} \tag{1}$$

where I is the total number of received frames, $h_{m,n}$ is the channel gain between the emitter and the (m,n)-th receiver antenna for the i-th frame, $x(i)$ is the transmitted signal, and $n(i)$ is additive white Gaussian noise (AWGN) at the receiver. Also, α and β are defined as

$$\alpha = \left(\frac{2\pi d_x}{\lambda}\right)\cos\theta, \tag{2}$$

$$\beta = \left(\frac{2\pi d_y}{\lambda}\right)\sin\theta\cos\phi, \tag{3}$$

where λ represents the emitter's signal wavelength, θ denotes the azimuth DoA by the far-field emitter measured with respect to the z-axis, and ϕ denotes its elevation DoA measured on the x-y plane. The i-th received frame across all the $M \times N$ antennas, $\mathbf{Y}(i) \in \mathbb{C}^{M\times N}$, is defined as

$$\mathbf{Y}(i) = h_{m,n}x(i)\mathbf{S}(\alpha,\beta) + \mathbf{N}(i), \quad i = 1,\ldots,I \tag{4}$$

where $\mathbf{S}(\alpha,\beta) = \mathbf{a}\mathbf{b}^T \in \mathbb{C}^{M\times N}$. Moreover, $\mathbf{a}(\alpha) \in \mathbb{C}^{M\times 1}$ and $\mathbf{b}(\beta) \in \mathbb{C}^{N\times 1}$ denote the steering vectors, defined as

$$\mathbf{a} = \left[1, e^{j\alpha}, \cdots, e^{j(M-1)\alpha}\right]^T, \tag{5}$$

$$\mathbf{b} = \left[1, e^{j\beta}, \cdots, e^{j(N-1)\beta}\right]^T, \tag{6}$$

and $\mathbf{N} \in \mathbb{C}^{M\times N}$ denotes the AWGN matrix.

3. PROPOSED METHOD

Given the URA, we propose to perform independent azimuth and elevation DoA estimation from a single received antenna array snapshot $\mathbf{Y}(i) \in \mathbb{C}^{M\times N}$. We define the complex mean vectors

$$\bar{\mathbf{y}}_{az} \in \mathbb{C}^{N\times 1} \text{ and } \bar{\mathbf{y}}_{el} \in \mathbb{C}^{M\times 1} \tag{7}$$

as the mean is taken over the real and imaginary parts of each row of $\mathbf{Y}$, $\mathbf{y}_{m,:}$, for $m = 1,\ldots,M$, and of each column of $\mathbf{Y}$, $\mathbf{y}_{:,n}$, for $n = 1,\ldots,N$, respectively. To harness the power of modern advancements in the broad field of linear algebra and in particular SVD, we "Hankelize" independently $\bar{\mathbf{y}}_{az}$ and $\bar{\mathbf{y}}_{el}$ to form a Hankel matrix; i.e., a matrix with constant value anti-diagonals [12]. For selected window parameters D_{az}, $2 \le D_{az} < N$ and $W_{az} = N - D_{az} + 1$, we define the side-by-side block Hankel matrix, $\mathbf{Y_{az}} \in \mathbb{R}^{D_{az}\times(2W_{az})}$ corresponding to $\bar{\mathbf{y}}_{az}$ as

$$\mathbf{Y_{az}} = [\Re(H(\bar{\mathbf{y}}_{az}))_{D_{az}\times W_{az}}, \Im(H(\bar{\mathbf{y}}_{az}))_{D_{az}\times W_{az}}] \tag{8}$$

where $H(\cdot)$ represents the "Hankelization" operator and $\Re(\cdot)$ and $\Im(\cdot)$ are the matrix operators that extract element-wise the real and imaginary parts of a matrix respectively. In the same direction, for selected window parameters D_{el}, $2 \le D_{el} < M$ and $W_{el} = M - D_{el} + 1$, we define the side-by-side block Hankel matrix $\mathbf{Y_{el}} \in \mathbb{R}^{D_{el}\times(2W_{el})}$, corresponding to $\bar{\mathbf{y}}_{el}$ as

$$\mathbf{Y_{el}} = [\Re(H(\bar{\mathbf{y}}_{el}))_{D_{el}\times W_{el}}, \Im(H(\bar{\mathbf{y}}_{el}))_{D_{el}\times W_{el}}]\,. \tag{9}$$

Subsequently, we perform rank-k decomposition of $\mathbf{Y_{az}}$ and $\mathbf{Y_{el}}$ using standard SVD to produce their corresponding k-rank representations

$$\tilde{\mathbf{Y}}_{az} = \mathbf{U}_{D_{az}\times k_{az}}\mathbf{\Sigma}_{k_{az}\times k_{az}}\mathbf{V}^T_{k_{az}\times 2W_{az}}, \tag{10}$$

$$\tilde{\mathbf{Y}}_{el} = \mathbf{U}_{D_{el}\times k_{el}}\mathbf{\Sigma}_{k_{el}\times k_{el}}\mathbf{V}^T_{k_{el}\times 2W_{el}}. \tag{11}$$

Thereafter, we force Hankelization by replacing all the anti-diagonals of $\tilde{\mathbf{Y}}_{az}$ and $\tilde{\mathbf{Y}}_{el}$ with their corresponding mean, and we extract the corresponding filtered azimuth and elevation vectors, $\tilde{\bar{\mathbf{y}}}_{az} \in \mathbb{C}^{N\times 1}$ and $\tilde{\bar{\mathbf{y}}}_{el} \in \mathbb{C}^{M\times 1}$ as a first-column last-row readout. Finally, we carry out matched-filter scanning for θ and ϕ:

$$\hat{\theta} = \arg\max_{\omega\in[-90^\circ,90^\circ)} \left|\tilde{\bar{\mathbf{y}}}^{\mathrm{H}}_{az}\mathbf{s}(\omega)\right|^2, \tag{12}$$

$$\hat{\phi} = \arg\max_{\omega\in[-90^\circ,90^\circ)} \left|\tilde{\bar{\mathbf{y}}}^{\mathrm{H}}_{el}\mathbf{s}(\omega)\right|^2 \tag{13}$$

where $\mathbf{s}(\omega)$ denotes the scanning vector that operates across the whole -90° to 89° continuum. The proposed algorithm is summarized in Fig. 2.

4. DATASETS

As part of the performance evaluation, we use both real signal measurements from the POWDER-RENEW massive MIMO testbed [13] and simulated data. We provide the source code for preparing the data for public access [14]. In this section, we discuss these data sources and, in the case of the massive MIMO dataset, discuss its topology, configurations, and calibration steps taken to prepare measurements for DoA estimation.

4.1. Simulation Measurements

Simulation data is generated to evaluate the proposed DoA estimation approach and to compare it with the state-of-the-art MUSIC algorithm under Rayleigh fading wireless channel conditions. The received signal is being augmented with additive white gaussian noise $n(i) \sim \mathcal{CN}(0, 1)$. Simulation data are generated using system parameters that are identical to the POWDER-RENEW massive MIMO testbed (e.g., carrier frequency, antenna spacing, number of antennas), described in Section 4.2. It is also important to note that the input to the algorithm is generated independently for azimuth and elevation DoA estimation cases.

4.2. Real Measurements

The experimental setup of the massive MIMO testbed is described below. The testbed is configured in an anechoic chamber. Two types of transmitters are used: a reference emitter and a client emitter. Both transmit repetitions of OFDM pilot frames. The reference emitter is statically positioned in front of the URA at a fixed height with an azimuth DoA of 0° and an elevation angle of -85°. The client emitter locations are changing across eight positions in the x-y plane and ten heights in the z plane. We consider all horizontal positions for the client emitter, but we limit our evaluation to a single elevation angle. However, since the distance of the client emitter from the receiver varies across locations, its elevation angle changes, too.

The receiver is a massive MIMO base-station with a total of 48 antenna elements positioned as a uniform rectangular array of six rows and eight columns of antennas. Since adjacent antenna pairs in the setup have different polarities, we only consider a sub-array of 6×4 antennas for our experimental evaluation. OFDM pilot frames are transmitted at a carrier frequency of 3.55 GHz. For each client position, pilot frames from the reference emitter precede frames from the client. Each transmitted pilot frame contains 27 long training symbols (LTS).

Proposed Algorithm: Hankel SVD Matched-Filtering

Input: Single received sample $\mathbf{Y} \in \mathbb{C}^{M \times N}$

1: Calculate complex mean vector $\bar{\mathbf{y}}_{az} \in \mathbb{C}^{N \times 1}$, $\bar{\mathbf{y}}_{el} \in \mathbb{C}^{M \times 1}$ (Eq. 7)

2a: Form side-by-side block Hankel matrix $\mathbf{Y_{az}}$ (Eq. 8)

2b: Form side-by-side block Hankel matrix $\mathbf{Y_{el}}$ (Eq. 9)

3a: For rank k_{az} decompose $\mathbf{Y}_{az}$ to $\mathbf{U}_{D_{az} \times k_{az}} \mathbf{\Sigma}_{k_{az} \times k_{az}} \mathbf{V}^T_{k_{az} \times 2W_{az}}$ (Eq.10)

3b: For rank k_{el} decompose $\mathbf{Y}_{el}$ to $\mathbf{U}_{D_{el} \times k_{el}} \mathbf{\Sigma}_{k_{el} \times k_{el}} \mathbf{V}^T_{k_{el} \times 2W_{el}}$ (Eq.11)

4a: Extract $\tilde{\bar{\mathbf{y}}}_{az}$ from mean Hankelized $\tilde{\mathbf{Y}}_{az}$

4b: Extract $\tilde{\bar{\mathbf{y}}}_{el}$ from mean Hankelized $\tilde{\mathbf{Y}}_{el}$

5a: Estimate $\hat{\theta}$ (Eq. 12)

5b: Estimate $\hat{\phi}$ (Eq. 13)

Output: $\hat{\theta}, \hat{\phi}$

Fig. 2: Summary of the proposed single-sample DoA algorithm using Hankel SVD matched-filtering for azimuth and elevation DoA estimation.

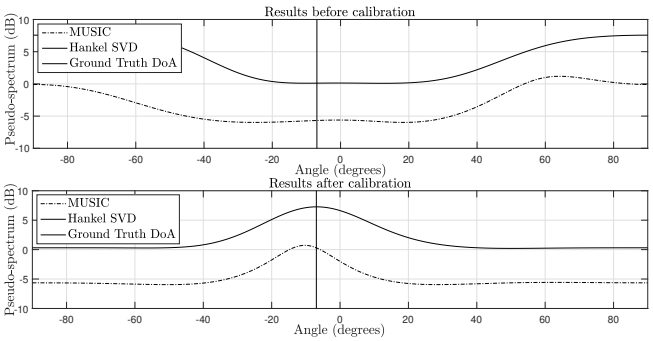

Fig. 3: The impact of inter-antenna calibration to DoA estimation carried out by standard MUSIC and the proposed single-sample DoA estimator.

The data calibration [9, 10] process comprises the following steps. We first eliminate carrier frequency offsets by determining phase shifts between two consecutive LTS from each antenna and each frame collected from the reference emitter. Estimated phase offsets are then applied to the whole frame, which reduces the impact of micro-Doppler effects in the measurements. Sampling time offsets are removed by finding the indices that correspond to the beginning of each LTS block for each frame and antenna. Here, we use an out-of-the-box method provided by the POWDER-RENEW testbed toolkit [13], which uses a priori known LTS sequence values at the receiver to find the beginning of each of the LTS blocks contained in the frame. Upon timing synchronization, LTS samples are extracted from frames for processing. Inter-antenna phase offset calibration requires additional data. Since these offsets are semi-deterministic [10], they can be estimated once every time the receiver hardware reboots. However, this is challenged by the absence of measurements collected in a wired setup, similar to an approach described in [8]. We address this challenge by leveraging frames transmitted from the reference emitter.

Wireless data from the reference emitter limits our capacity to estimate inter-antenna phase offsets perfectly. However, these results allow us to considerably improve the performance of both MUSIC and the proposed single-sample DoA estimator. Figure 3 shows the performance of both DoA estimation algorithms before and after data calibration for the reference emitter. For each method, we plot the pseudo-spectrum output of each algorithm on a logarithmic scale. We observe clearly the improvement in DoA estimation achieved by both algorithms after data calibration.

5. PERFORMANCE EVALUATION

Considering both simulation and real data measurements, we compare the performance of MUSIC and the proposed Hankel SVD algorithm under two distinct scenarios. First, we apply both algorithms using all the available samples per frame i.e., MUSIC produces one DoA estimate per frame while Hankel SVD produces a DoA estimate for every single sample in the frame. Second, we match-filter the incoming signal with the DoA steering vector scanning across the whole $-90°$ to $89°$ continuum and select samples that produce an absolute DoA estimation error below a pre-defined threshold.

We first compare the performance of MUSIC and the

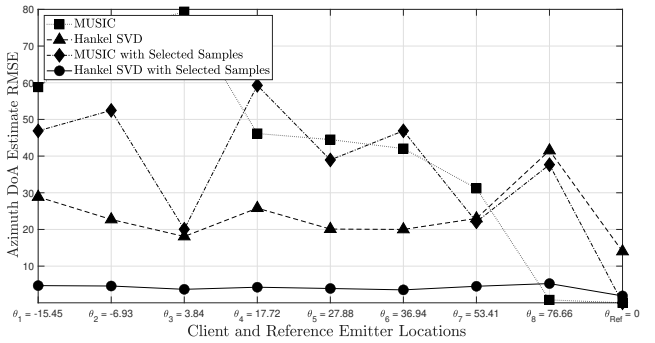

(a) Azimuth DoA

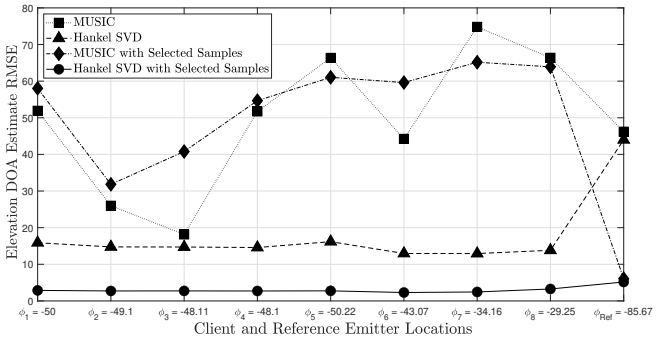

(b) Elevation DoA

Fig. 4: RMSE performance of the proposed method vs MUSIC on simulation data.

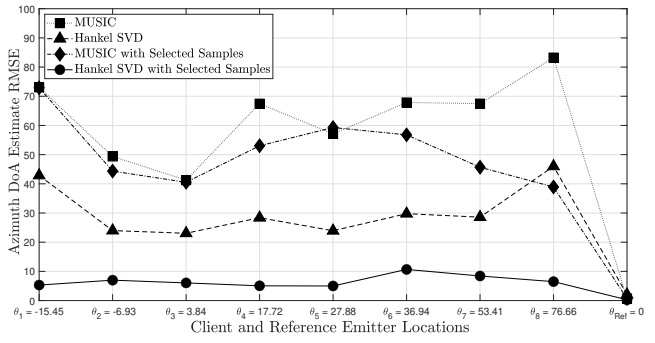

(a) Azimuth DoA

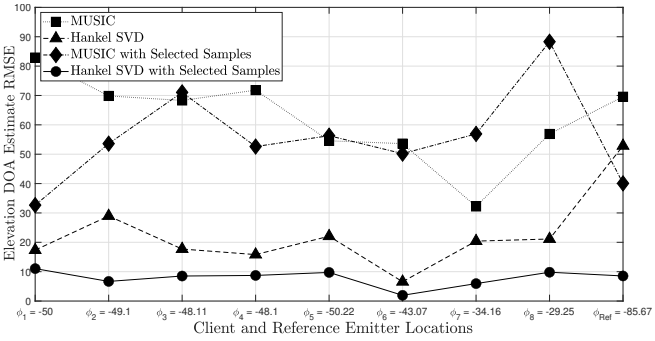

(b) Elevation DoA

Fig. 5: RMSE performance of the proposed method vs MUSIC on real measurements from POWDER-RENEW.

proposed Hankel SVD algorithm on the simulation data described in Section 4.1. The results for both techniques are illustrated in Fig. 4a and 4b. The x-axis denotes the index and true DoA of the emitting device, while the y-axis denotes the root mean square error (RMSE) between the estimated and true DoA estimated by the massive MIMO receiver in degrees. It is important to note that the rank and window selection parameters of the Hankel SVD algorithm have been optimized experimentally.

For the first scenario, MUSIC uses all samples available in each received frame to form an appropriate estimate of the space-domain signal autocorrelation matrix. More specifically, it uses 128 samples per frame to calculate a DoA estimate, while the proposed algorithm produces a DoA estimate for a single array snapshot (i.e. 128 DoA estimates for each frame). As a result, for the proposed method, we calculate RMSE by averaging all 128 DoA estimates per frame over the 20 frames used for experimental evaluation, whereas MUSIC RMSE is calculated by averaging DoA estimates (one per frame) over 20 frames. While the Hankel SVD method performs better compared to MUSIC for azimuth and elevation in almost all cases and alleviates the spatial aliasing problem, both approaches record a relatively high RMSE which deems them practically inapplicable. This observation motivated us in the second scenario to select samples that have absolute estimation error below a pre-defined threshold of 15 degrees. In this case, the proposed method consistently outperforms its counterpart, MUSIC for all emitter locations.

We then evaluate both algorithms on real measurements. The results are illustrated in Fig. 5a and Fig. 5b. Similarly, the x-axis denotes the index and true DoA of the emitting device, while the y-axis depicts RMSE measured in degrees. The performance of the proposed Hankel SVD method consistently outperforms MUSIC DoA estimation results, confirming in practice our simulation results. Here, we specifically observe that the quality of MUSIC DoA estimates is considerably affected by data calibration (that is not taken into account during simulation) and spatial aliasing. As described in the previous section, since data calibration cannot entirely mitigate inter-antenna phase offsets, the effects of calibration remain volatile across frames. Yet, experimental results show that the proposed Hankel SVD algorithm can consistently mitigate calibration and aliasing impairments.

6. CONCLUSIONS

Modification of radio sensing hardware (especially in large-scale MIMO) configurations for localization is often a challenge. This becomes apparent when, for example, inter-antenna spacing requirements cannot match transmission frequency configurations. In this paper, we evaluated on real measurements from a massive MIMO testbed the extreme case of signal DoA estimation from just a single antenna array snapshot. Experimental results confirmed our simulations and showed that the proposed DoA estimation algorithm withstands errors due to spatial aliasing and imperfect data calibration, while the performance of state-of-the-art subspace-based methods is significantly degraded. The proposed method could be the foundation for continued development of fast and high-accuracy location-based services for smart urban city environments.

7. REFERENCES

[1] Chenglong Li, Sibren De Bast, Emmeric Tanghe, Sofie Pollin, and Wout Joseph, "Toward fine-grained indoor localization based on massive MIMO-OFDM system: Experiment and analysis," *IEEE Sensors Journal*, vol. 22, no. 6, pp. 5318–5328, 2022.

[2] Xuhong Li, Erik Leitinger, Magnus Oskarsson, Kalle Åström, and Fredrik Tufvesson, "Massive MIMO-based localization and mapping exploiting phase information of multipath components," *IEEE Transactions on Wireless Communications*, vol. 18, no. 9, pp. 4254–4267, 2019.

[3] Ming-Yang Cao, Xingpeng Mao, Xiaozhuan Long, and Lei Huang, "Direction-of-arrival estimation for uniform rectangular array: A multilinear projection approach," in *2018 26th European Signal Processing Conference (EUSIPCO)*. IEEE, 2018, pp. 1237–1241.

[4] Ningjun Ruan, Han Wang, Fangqing Wen, and Junpeng Shi, "DoA estimation in B5G/6G: Trends and challenges," *Sensors*, vol. 22, no. 14, pp. 5125, 2022.

[5] Kai-Yu Yang, Jwo-Yuh Wu, and Wen-Hsuan Li, "A low-complexity direction-of-arrival estimation algorithm for full-dimension massive MIMO systems," in *2014 IEEE International Conference on Communication Systems*. IEEE, 2014, pp. 472–476.

[6] Ralph Schmidt, "Multiple emitter location and signal parameter estimation," *IEEE transactions on antennas and propagation*, vol. 34, no. 3, pp. 276–280, 1986.

[7] Navid Tadayon, Muhammed Tahsin Rahman, Shuo Han, Shahrokh Valaee, and Wei Yu, "Decimeter ranging with channel state information," *IEEE Transactions on Wireless Communications*, vol. 18, no. 7, pp. 3453–3468, 2019.

[8] Anatolij Zubow, Piotr Gawłowicz, and Falko Dressler, "On phase offsets of 802.11 ac commodity WiFi," in *2021 16th Annual Conference on Wireless On-demand Network Systems and Services Conference (WONS)*. IEEE, 2021, pp. 1–4.

[9] George Karystinos, "Secure communication based on robust 3D localization," https://ngiatlantic.eu/funded-experiments/secure-communication-based-robust-3d-localization, 2022.

[10] Dongheng Zhang, Yang Hu, Yan Chen, and Bing Zeng, "Calibrating phase offsets for commodity WiFi," *IEEE Systems Journal*, vol. 14, no. 1, pp. 661–664, 2019.

[11] Georgios I. Orfanidis, Dimitris A. Pados, George Sklivanitis, Elizabeth S. Bentley, Joseph Suprenant, and Michael J. Medley, "Single-sample direction-of-arrival estimation by hankel-matrix decompositions," in *Asilomar Conf. Signals, Syst. Comput.* IEEE, 2022, pp. 1026–1030.

[12] Georgios I. Orfanidis, Dimitris A. Pados, and George Sklivanitis, "Time-series analysis with small and faulty data: L1-norm decompositions of hankel matrices," in *Big Data IV: Learning, Analytics, and Applications*. SPIE, 2022, vol. 12097, pp. 97–104.

[13] Joshua Miraglia, "POWDER Massive MIMO repository," https://gitlab.flux.utah.edu/cnn-signal-discovery-senior-project/signal-collection, 2022.

[14] Stepan Mazokha, Sanaz Naderi, Georgios I. Orfanidis, George Sklivanitis, Dimitris A. Pados, and Jason O. Hallstrom, "Single-sample direction-of-arrival estimation for fast and robust 3D localization with real measurements from a massive MIMO system," https://github.com/C2A2-at-Florida-Atlantic-University/icasp_single_sample_doa_estimation, 2023.